JOURNAL OF GEOPHYSICAL RESEARCH: ATMOSPHERES, VOL. 118, 1–17, doi:10.1002/jgrd.50204, 2013

Reassessing the variability in atmospheric H_2 using the two-way nested TM5 model

G. Pieterse,[1] M. C. Krol,[1,2] A. M. Batenburg,[1] C. A. M. Brenninkmeijer,[3]
M. E. Popa,[1,4] S. O'Doherty,[5] A. Grant,[5] L. P. Steele,[6] P. B. Krummel,[6]
R. L. Langenfelds,[6] H. J. Wang,[7] A. T. Vermeulen,[4] M. Schmidt,[8] C. Yver,[8]
A. Jordan,[9] A. Engel,[10] R. E. Fisher,[11] D. Lowry,[11] E. G. Nisbet,[11] S. Reimann,[12]
M. K. Vollmer,[12] M. Steinbacher,[12] S. Hammer,[13] G. Forster,[14]
W. T. Sturges,[14] and T. Röckmann[1]

Received 6 April 2012; revised 12 January 2013; accepted 15 January 2013.

[1] This work reassesses the global atmospheric budget of H_2 with the TM5 model. The recent adjustment of the calibration scale for H_2 translates into a change in the tropospheric burden. Furthermore, the ECMWF Reanalysis-Interim (ERA-Interim) data from the European Centre for Medium-Range Weather Forecasts (ECMWF) used in this study show slower vertical transport than the operational data used before. Consequently, more H_2 is removed by deposition. The deposition parametrization is updated because significant deposition fluxes for snow, water, and vegetation surfaces were calculated in our previous study. Timescales of 1–2 h are asserted for the transport of H_2 through the canopies of densely vegetated regions. The global scale variability of H_2 and $\delta D[H_2]$ is well represented by the updated model. H_2 is slightly overestimated in the Southern Hemisphere because too little H_2 is removed by dry deposition to rainforests and savannahs. The variability in H_2 over Europe is further investigated using a high-resolution model subdomain. It is shown that discrepancies between the model and the observations are mainly caused by the finite model resolution. The tropospheric burden is estimated at 165 ± 8 Tg H_2. The removal rates of H_2 by deposition and photochemical oxidation are estimated at 53 ± 4 and 23 ± 2 Tg H_2/yr, resulting in a tropospheric lifetime of 2.2 ± 0.2 year.

Citation: Pieterse, G., et al. (2013), Reassessing the variability in atmospheric H_2 using the two-way nested TM5 model, *J. Geophys. Res. Atmos.*, *118*, doi:10.1002/jgrd.50204.

1. Introduction

[2] Since the industrialization of fuel cell technology during the 1970s and 1980s, molecular hydrogen (H_2) has been considered as a clean alternative for fossil fuel based energy carriers. The selective oxidation of H_2 by oxygen only produces water, contrary to the combustion of fossil fuels with air that produces carbon dioxide, carbon monoxide, nitrogen oxides, soot, and many other volatile organic compounds. As H_2 is not readily available in large quantities, practical applications of fuel cell technology rely on conversion from other energy carriers (e.g., bio fuels or fossil fuels) or generation of H_2 from direct energy sources (e.g., solar

[1]Institute for Marine and Atmospheric Research Utrecht (IMAU), Utrecht, The Netherlands.
[2]Department of Meteorology and Air Quality at Wageningen University, Wageningen, The Netherlands.
[3]Max-Planck-Institut für Chemie, Air Chemistry Division, Mainz, Germany.
[4]Department of Air Quality and Climate Research at the Energy Research Centre of the Netherlands (ECN), Petten, The Netherlands.
[5]School of Chemistry, University of Bristol, Bristol, UK.
[6]Centre for Australian Weather and Climate Research, CSIRO Marine and Atmospheric Research, Aspendale, Victoria, Australia.
[7]School of Earth and Atmospheric Sciences, Georgia Institute of Technology, Atlanta, GA, USA.
[8]Laboratoire des Sciences du Climat et de l'Environnement (LSCE), Gif-sur-Yvette, France.
[9]Max-Planck Institut für Biogeochemie, Jena, Germany.
[10]Institut für Meteorologie und Geophysik, Goethe-Universität Frankfurt, Frankfurt, Germany.

Corresponding author: G. Pieterse, Institute for Marine and Atmospheric Research Utrecht (IMAU), Princetonplein 5, 3584 CC, Utrecht, The Netherlands. (Gerben_Pieterse@hotmail.com)

2169-897X/13/10.1002.50204

[11]Department of Earth Sciences, Royal Holloway, University of London, Egham, UK.
[12]Empa, Swiss Federal Institute for Materials Science and Technology, Laboratory for Air Pollution/Environmental Technology, Duebendorf, Switzerland.
[13]Institut für Umweltphysik, Heidelberg Universität, Heidelberg, Germany.
[14]School of Environmental Sciences, University of East Anglia, Norwich, UK.

energy). The low overall well-to-wheel efficiency of the entire energy production chain and the accompanying costs have so far limited the use of H_2 to a relatively small number of applications. Nevertheless, the potential for improving urban air quality and reducing the human impact on climate remains appealing. The positive effects of H_2 usage on air quality and climate might be accompanied by adverse effects. Scaling up the use of H_2 might lead to an increasing input of H_2 into the atmosphere and, thus, to a larger atmospheric burden of H_2. Enhanced levels of H_2 might prolong the atmospheric life time of the greenhouse gas methane and increase its effect on climate [*Schultz et al.*, 2003]. Methane and H_2 are both removed from the atmosphere via chemical oxidation by the hydroxyl (OH) radical. Higher levels of H_2 would consume more OH radicals and herewith reduce the photochemical destruction of CH_4. As the oxidation of H_2 produces water [*Tromp et al.*, 2003; *Warwick et al.*, 2004; *Feck et al.*, 2008], increasing H_2 mixing ratios in the stratosphere might also enhance the formation of polar stratospheric clouds. This in turn can result in increased chlorine activation and subsequent loss of ozone during the polar spring, although the effect is probably small in view of the variability of stratospheric water vapor [*Vogel et al.*, 2012].

[3] A good understanding of the present-day global H_2 cycle is a prerequisite to anticipate any adverse effects as a result of additional H_2 emissions that can be expected from a more intensified use as an energy carrier. Observations of atmospheric H_2 mixing ratios were only scarcely available until the Global Monitoring Division (GMD), nowadays the Earth System Research Laboratory (ESRL), at the National Oceanic and Atmospheric Administration (NOAA) started systematic flask measurements at five sites in 1989, increasing to 52 sites during the 1990s. Additional data have been generated for 11 sites since the early 1990s by the Commonwealth Scientific and Industrial Research Organisation (CSIRO) [*Francey et al.*, 1996; *Langenfelds et al.*, 2002; *Jordan and Steinberg*, 2011]. The results from the NOAA/ESRL network have been analyzed extensively by *Novelli et al.* [1999] and translated to a global budget. H_2 is emitted into the atmosphere due to the usage of fossil fuels, by biomass burning, and as a reaction product of nitrogen fixation processes in the soils and oceans. Furthermore, it is photochemically produced from CH_4 and nonmethane hydrocarbons (NMHCs). H_2 is removed from the atmosphere by photochemical reaction with OH and by dry deposition to the soils. The values of the magnitudes of the sources and sinks reported by *Novelli et al.* [1999] are still supported by most recent studies, but the uncertainties remain large [*Hauglustaine and Ehhalt*, 2002; *Sanderson et al.*, 2003; *Rhee et al.*, 2006; *Price et al.*, 2007; *Xiao et al.*, 2007; *Ehhalt and Rohrer*, 2009; *Pison et al.*, 2009; *Yver et al.*, 2011; *Bousquet et al.*, 2011; *Pieterse et al.*, 2011; *Yashiro et al.*, 2011]. Two of these studies [*Rhee et al.*, 2006; *Xiao et al.* 2007] report a significantly larger contribution of the main sink of H_2, i.e., dry deposition, to the global budget than all others.

[4] In a number of the above-mentioned studies, three-dimensional chemical transport models (CTMs) were used to study the global and regional H_2 cycles [*Hauglustaine and Ehhalt*, 2002; *Sanderson et al.*, 2003; *Yashiro et al.*, 2011] by means of comparison with available measurements of H_2 mixing ratios. *Pison et al.* [2009], *Yver et al.* [2011] and *Bousquet et al.* [2011] used atmospheric observations of H_2 mixing ratios and other species to determine the magnitudes of the source and sink processes by means of a Bayesian inverse modeling approach adopted from *Bousquet et al.* [2005]. In order to further constrain the global H_2 budget, *Price et al.* [2007] implemented the sources and sinks for the singly deuterated stable H_2 isotopologue (HD) assuming a fixed ratio between the photochemical production of H_2 and HD. Modeled and measured isotopic compositions of molecular hydrogen are all calculated from the ratio $R = D/H$ as $\delta D[H_2] = (R/R_{VSMOW} - 1)$, where $R_{VSMOW} = 1.558 \times 10^{-4}$ is the reference D/H ratio of Vienna Standard Mean Ocean Water (VSMOW). The resulting framework was also used to evaluate the stable H_2 isotope budgets previously reported by *Gerst and Quay* [2001], *Rahn et al.* [2002], *Rahn et al.* [2003], and *Rhee et al.* [2006]. A full H_2 isotope chemistry scheme was recently implemented in the TM5 model [*Pieterse et al.*, 2009, 2011] and used to further constrain the global budget of H_2 with $\delta D[H_2]$ measurements. Both studies showed that the modeled tropospheric $\delta D[H_2]$ is very sensitive to the values of the isotopic composition of stratospheric molecular hydrogen that is heavily enriched in deuterium [*Rahn et al.*, 2003; *Röckmann et al.*, 2003]. This sensitivity suggests an important role of the stratosphere troposphere exchange (STE) for the tropospheric HD budget and stresses the importance of using an appropriate stratospheric chemistry scheme or correct boundary condition.

[5] The objective of this study is to further constrain the global H_2 budget by comparing model results to measured H_2 mixing ratios and isotopic compositions and by using the ratio between photochemical production of H_2 and CO as an additional constraint. For the first time, we compare our model results to high temporal resolution H_2 measurements from the EuroHydros project [*Engel and EUROHYDROS PIs*, 2009]. The hourly H_2 mixing ratios measured at these stations are used to evaluate the modeled H_2 mixing ratios. Additionally, the values of $\delta D[H_2]$ in air collected at five flask sampling sites during the EuroHydros project [*Batenburg et al.*, 2011] are used to evaluate the model results. A further constraint is provided by the isotopic composition of air samples collected in the upper troposphere and the lower stratosphere by the CARIBIC (Civil Aircraft for the Regular Investigation of the Atmosphere Based on an Instrument Container) program [*Brenninkmeijer et al.* 2007; *Batenburg et al.*, 2012].

[6] The required changes to match the TM5 model results with the new observations are described in section 2, along with the recent update of the calibration scale for H_2 measurements [*Jordan and Steinberg*, 2011] adopted by the World Meteorological Organisation (WMO) and an update of the H_2 deposition scheme to correct for a previous overestimated deposition to wet and snow surfaces. Section 3 starts with an evaluation of modeled global and latitudinal variability in H_2 and $\delta D[H_2]$ in sections 3.1 and 3.2, respectively. Subsequently, the regional scale model performance is evaluated in section 3.3 by means of a wind sector analysis for a selection of stations from the EuroHydros project. Section 4 proceeds by discussing the implications of the study for the global

H_2 budget, and the overall conclusions are summarized in section 5.

2. Methods

[7] The two-way nested setup of the TM5 model [*Krol et al.*, 2005] was recently enhanced by implementing a H_2 isotope chemistry scheme [*Pieterse et al.*, 2009], an H_2 emission inventory adopted from the project for Global and regional Earth system Monitoring using Satellite and in situ data [GEMS: *Schultz and Stein*, 2006], a soil moisture dependent deposition parametrization [*Sanderson et al.*, 2003], and a stratospheric parametrization for H_2 and HD [*Rahn et al.*, 2003; *McCarthy et al.*, 2004; *Pieterse et al.*, 2011]. Our previous study [*Pieterse et al.*, 2011] was primarily focussed on the introduction and global evaluation of the new H_2 isotope chemistry scheme. Therefore, the global and latitudinal variability in H_2 were investigated using a single global model domain with a resolution of 6 by 4 degrees in the longitudinal and latitudinal directions, respectively. In this study, the model performance is also evaluated for a model subdomain with a resolution of 1 by 1 degrees over Europe.

2.1. Surface Emissions of H_2

[8] In GEMS, the emissions related to fossil fuel use are separated into five categories: power generation; industrial combustion; road transport; an aggregated emission category that includes residential, commercial, and other combustion processes [*Schaap et al.*, 2005; *Schultz et al.* 2007], and emissions related to marine traffic [*Endresen et al.*, 2003]. The GEMS emissions due to biomass burning originate from a variety of sources such as wild fires, deforestation fires, bio fuel burning, agricultural waste burning, peat burning, and charcoal production/burning [*Andreae and Merlet*., 2001; *Christian et al*., 2003; *van der Werf et al*., 2003, 2010]. The spatial and temporal variability of the GEMS H_2 emissions from the ocean due to N_2 fixation are adopted from the spatial and temporal distributions of CO from the oceans [*Erickson and Taylor*, 1992]. The CO emissions are believed to be a robust indicator for the presence of biological activity and therefore also for the presence of N_2 fixing microbial species such as Cyanobacteria. Similarly, the geographical distribution of biogenic CO emissions given by *Müller* [1992] is used to describe the spatial variability of emissions due to N_2 fixation on the continents by Rhizobia. Just as in *Pieterse et al.* [2011], the different source fluxes, originally derived for the year 2003, are scaled to the average of previously reported global budget estimates [*Novelli et al.*, 1999; *Hauglustaine and Ehhalt*, 2002; *Sanderson et al.*, 2003; *Rhee et al.*, 2006; *Price et al.*, 2007; *Xiao et al.* 2007; *Ehhalt and Rohrer*, 2009; *Yashiro et al.*, 2011]. With the resulting model framework, the global tropospheric cycle of H_2 and $\delta D[H_2]$ can be investigated along with 29 other chemical tracers implemented in the Carbon Bond Mechanism, version 4 [CBM-4, *Gery et al*., 1988, 1989; *Houweling et al*., 1998]. This feature can be used for imposing multispecies constraints upon the global budget of H_2. In the following analysis, H_2 mixing ratios, isotopic compositions, and the known photochemical source magnitude of CO are used to constrain the H_2 budget.

2.2. Measurement Data Used for This Study

[9] Model values for the H_2 mixing ratios are compared with available data from a subset of stations from the EuroHydros project [*Engel and EUROHYDROS PIs*, 2009] within the high-resolution zoom region over Europe, namely Mace Head (Ireland) [*Grant et al*., 2010], London (United Kingdom) [*Fowler et al*., 2011], Weybourne (United Kingdom), Cabauw (The Netherlands) [*Popa et al*., 2011], Gif-sur-Yvette (France) [2009, 2011], Taunus (Germany), Heidelberg (Germany) [*Hammer and Levin*, 2009], Jungfraujoch (Switzerland) [*Bond et al*., 2011], and Bialystok (Poland); see Figure 6. The global scale performance for the H_2 mixing ratios is evaluated using flask sampling data from the CSIRO network measured at Alert (Canada), Cape Ferguson (Australia), Cape Grim (Australia), Casey Station (Antarctica), Macquarie Island (Australia), Mauna Loa (United States), Mawson (Antarctica), and the South Pole. For the global scale comparisons, the model results and continuous measurements are sampled between 11 A.M. and 1 P.M. local time. This way, the inherent discrepancies between the modeled values and the measurements due to subgrid level variability (the representation errors) and local influences are suppressed. Generally, the strongest vertical mixing occurs during this time of the day, and measurements are thus less influenced by local soil uptake or local sources. The noontime values are therefore more representative for the large spatial and temporal scales. The latitudinal gradients in $\delta D[H_2]$ are investigated using existing data collected during ship measurement campaigns [*Gerst and Quay*, 2000; *Rice et al.*, 2010] and novel data from the EuroHydros project measured at Alert, Mace Head, Cape Verde, Amsterdam Island (France), and the South Pole [*Batenburg et al.*, 2011].

2.3. Meteorological Data Used for This Study

[10] In *Pieterse et al.* [2011], operational data from the European Centre for Medium-Range Weather Forecasts (ECMWF) were used for the simulations. In this work, ECMWF Reanalysis-Interim (ERA-Interim) data are employed. These data show less vertical motion which leads to much steeper surface gradients in the modeled H_2 mixing ratios. As will be shown in the result sections, this leads to a significant reduction in the modeled tropospheric burden of H_2. It is not straightforward to determine which meteorological data are closest to reality for the time period between 2007 and 2008. The overview in *Dee et al.* [2011] shows that the operational and ERA-Interim model versions were the same at the start of the year 2007. Nevertheless, several updates were implemented in the operational model between 2007 and 2008. This leads to inconsistencies in the operational data for long-term simulation periods, and therefore, we prefer to use the ERA-Interim data in this work. Interestingly, the H_2 budget appears very sensitive to large-scale vertical transport, and an update of our previous implementation is required.

2.4. Update of the New WMO Calibration Scale for H_2 Mixing Ratios

[11] *Jordan and Steinberg* [2011] proposed a new Global Atmospheric Watch (GAW) H_2 mole fraction calibration scale. This MPI-2009 scale has recently been adopted by

the WMO. Converting the original values for the H_2 mixing ratios measured by CSIRO to the MPI-2009 scale will increase the values by 3.1% [*Jordan and Steinberg*, 2011]. The data from the EuroHydros project are already calibrated against the MPI-2009 scale. As a result of this change, it is expected that the original H_2 scheme, introduced in our previous study [*Pieterse et al.*, 2011] and verified by NOAA/ESRL and CSIRO data will underestimate the recalibrated measured H_2 mixing ratios.

2.5. Update of the Stratospheric Boundary Condition

[12] Because the TM5 model is primarily designed for tropospheric studies, the stratospheric isotope chemistry scheme is incomplete. For instance, reactions of chemical species with electronically excited oxygen (O^1D), chlorine (Cl), and bromine (Br) radicals are not implemented. Especially the reactions with Cl and Br introduce strong isotope effects in the CH_4 oxidation chain [*Feilberg et al.*, 2004; *Mar et al.*, 2007]. Therefore, a stratospheric boundary condition based on the parametrization introduced by *McCarthy et al.* [2004] was used in *Pieterse et al.* [2011]. Without this upper-boundary condition, the modeled tropospheric composition would be about +99‰. By forcing the HD mixing ratios in the lower stratosphere to observations according to the parametrization by *McCarthy et al.* [2004], the modeled tropospheric composition is enriched to +128‰. This correction is rather large in view of the small impact of the stratosphere on the tropospheric burden of H_2 and stresses the importance of using sufficiently representative empirical relations to define the boundary condition. Here, upper tropospheric/lower stratospheric measurements of $\delta D[H_2]$ from the CARIBIC program [*Brenninkmeijer et al.* 2007] recently published by *Batenburg et al.* [2012] are used to update the original relation between the CH_4 mixing ratio (units in ppb) and the isotopic composition of H_2 (units in ‰ versus VSMOW) in the stratosphere to the following:

$$\delta D[H_2] = -0.350[CH_4] + 768. \quad (1)$$

Because it is actually HD that is traced by the model, this relation is first transformed into a relation between HD and CH_4. The stratospheric H_2 mixing ratio was set to 545 ppb following the adjustment to the MPI-2009 calibration scale. This results in the following relation for HD (units in ppb):

$$[HD] = -7.585 \times 10^{-5}[CH_4] + 0.338. \quad (2)$$

The required values for the CH_4 mixing ratios are obtained from the four-dimensional variational (4D-Var) data assimilation system implemented in TM5 [*Meirink et al.*, 2008a, 2008b]. These CH_4 fields also drive the isotope chemistry scheme. Using the values that are calculated with these parametric expressions, the stratospheric H_2 mixing ratio is then obtained from the following expression (units in ppb):

$$[H_2] = \frac{1}{2(\delta D[H_2] + 1)R_{VSMOW}}[HD]. \quad (3)$$

The factor 2 accounts for the fact that the isotopic composition is measured at a per atom basis. Just as in *Pieterse et al.* [2011], the following latitude (θ) dependent threshold pressure level p_s (Pa) separates the troposphere and the stratosphere:

$$p_s = 3.00 \times 10^4 - 2.15 \times 10^4 \cos(\theta). \quad (4)$$

For all pressures below the threshold pressure level, the mixing ratios for H_2 and HD calculated by the default chemistry scheme are replaced by the empirical expressions that are described above. The model keeps track of the mass of H_2 and HD removed or added from or to the values obtained using the chemistry scheme. In this way, the stratospheric correction imposed by the stratospheric parametrization can be calculated for the model domain up to 100 mbar used for the global budget calculations presented in Table 3. The flux of H_2 and HD across the 100 mbar model boundary is referred to as the vertical flux.

2.6. Update of the Deposition Parametrization

[13] By analyzing the H_2 budget, it was found out that significant amounts of H_2 deposited on snow, oceans, and vegetation surfaces. In the default implementation that is implemented in TM5 [*van Pul and Jacobs*, 1994; *Ganzeveld and Lelieveld*, 1995; *Ganzeveld et al*., 1998], the large resistance values ($1 \cdot 10^5$ sm^{-1}) for deposition to these surfaces were still small enough to allow for significant amounts of H_2 deposition, with deposition velocities up to 0.01 mms^{-1}. As a result, H_2 was also removed at these surfaces, whereas in reality, biological processes are significantly suppressed in frozen environments, and H_2 hardly dissolves in water. Actually, *Lallo et al.* [2008] report small but nonzero deposition velocities to snow-covered soils at temperatures near the freezing point.

[14] Suppression of deposition to vegetation surfaces resulted in very little H_2 uptake in tropical forests, in contrast with the large deposition velocities that are typically measured in these regions. Therefore, the surface uptake parametrization was reevaluated. TM5 uses a canopy resistance model to represent the circulation of air within a canopy. This model was developed for deposition of ozone over maize crop by *Pul and Jacobs* [1994]. They derived the following empirical formula for the in-canopy resistance, R_i:

$$R_i = 14\frac{\mathrm{LAI}\, h_{can}}{u^*}. \quad (5)$$

In this expression, h_{can} (m) is the canopy height, LAI the leaf area index, u^* (ms^{-1}) the friction velocity, and 14 (m^{-1}) is an empirical factor. The expression is commonly used by many CTMs to calculate the impact of the vegetation canopies on the dry deposition of a given chemical species to the soils underneath [*Sanderson et al.*, 2003; *Price et al.*, 2007]. When applied to H_2, this parametrization leads to very low deposition over tropical rainforests and Savannah regions, whereas in previous experimental studies [*Conrad and Seiler*, 1985; *Yonemura et al.*, 2000], large deposition velocities were observed for these regions. Since H_2 does not deposit to plants, a high canopy aerodynamic resistance over rainforests ($O\left[10^4\right]$ sm^{-1} with LAI = 6, h_{can} = 30 m,

$u^* = 0.1\ ms^{-1}$) is therefore not realistic, since intermittent transport processes refresh the air in the canopy roughly every 1 to 2 h [*Ganzeveld et al.*, 2002; *Foken et al.* 2012]. Therefore, we will also investigate the impact of reducing the empirical factor to $0.1 m^{-1}$. In this case, the R_i still scales with LAI, h_{can}, and $1/u^*$ but for typical rainforest characteristics, this leads to a more realistic time scale of $R_i\, h_{can} = 5400$ s or 1.5 h for refreshing the air under the canopy. In the budget reported by *Sanderson et al.* [2003], the sources exceeded the sinks by of 4.1 Tg H_2/yr. This imbalance might have been caused by too little deposition. Because no deposition maps were reported by the authors, it was not possible to check for low deposition velocities above the rainforests. *Price et al.* [2007] replaced the default deposition parametrization by a constant deposition velocity. Hence, the in-canopy resistance was not used for their calculations. Because vegetation will affect the transport of species towards the soil below, we prefer to use a canopy resistance dependent on LAI, canopy height, and friction velocity rather than to use no resistance at all.

2.7. Definition of Scenario Studies to Reestablish a Closed H_2 Budget

[15] The results from seven different scenario simulations of the TM5 model are analyzed using data from the EuroHydros project. An overview of these scenarios is shown in Table 1. We will run these scenarios to examine the effect of changing individual source and sink terms in the global budget on the temporal and latitudinal distribution of H_2 and HD in the troposphere and compare the scenarios to available measurements. Preliminary calculations showed that the effect of removing the deposition pathways to snow, oceans, and wet vegetation surfaces is large. In order to reclose the H_2 budget, we must aim at a 14 Tg H_2/yr change in each of the most relevant sources and sinks. Subsequently, the model performance will be validated for all scenarios using the H_2 flask sampling data from CSIRO.

[16] In the reference scenario, hereafter referred to as S1, the default H_2 isotope scheme [*Pieterse et al.*, 2011] is used. This scenario will show the impact of the ERA-Interim meteorological data on the original model results. In the second scenario (S2), the suppression of deposition to snow and water surfaces, wetted surfaces, vegetation leaf surfaces, and leaf mesophyll tissue is evaluated. This way, the impact of the spurious deposition fluxes on the H_2 budget calculated by the original model are quantified. Note that in scenario S2, the total deposition velocities are no longer scaled to 90%, as was done in *Pieterse et al.* [2011] to balance the budget. For the third scenario (S3a), the in-canopy resistance for H_2 is decreased (see section 2.6). Since this scenario leads to a small overestimate for H_2 at the Antarctic stations, scenario S3b explores an additional reduction of 2 Tg H_2/yr ocean emissions due to N_2 fixation. In scenario S3c, the impact of increasing the deposition velocities for forest and Savannah ecosystem types by 10% in the SH H_2 mixing ratios and isotopic compositions is investigated as alternative scenario to decrease H_2 at high southern latitudes. Because the NH H_2 mixing ratios and isotopic compositions were already on par with the measurements, the deposition velocities to agricultural regions are decreased by 10% in scenario S3c to compensate for the increase in the deposition to forest regions.

[17] As the required adjustment for the tropospheric burden of H_2 is large compared to the magnitudes and ranges of uncertainty for the majority of the remaining sources and sinks in the H_2 budget, only two additional scenarios are explored to close the gap between the model results of scenario S2 (caused by the correct suppression of deposition to wet and snow surfaces) and the measurements. In scenario S4, the emissions of H_2 due to fossil fuel usage are reduced. It is noted that the adjustment required to close the gap caused by the correction of the deposition scheme (S2) is very large, but the effects are approximately linear so that the effect can be scaled to investigate smaller changes. With scenario S5, we attempt to close the budget by increasing the H_2 sink from OH oxidation. An increase of 53% in the rate constant is needed to achieve the required increase of 9.5 Tg H_2/yr in this sink term. This reduction is smaller than the required decrease for the sources because deposition scales with the burden of H_2. As a result, the relative contribution of the removal by deposition will increase with a decreasing overall burden, and therefore the required increase in the photochemical removal is reduced. However, scenario S5 is still considered unlikely because the rate constant for the photochemical removal of H_2 by OH is

Table 1. Overview of Scenarios Aiming at Closing the Global Budget of H_2 and $\delta D[H_2]$

Name	Explanation	Change in Budget Term[a]	Change in Burden[b]
S1	Different meteorology[c]	–	–1.9%
S2	Corrected deposition parametrization	–24.7%	+14.3%
S3a	Reduced in-canopy deposition resistance	–12.0%	+8.4%
S3b	Reduced in-canopy deposition resistance + Decreased ocean N_2 fixation emissions	–15.0% –40.0%	+7.1%
S3c	Adjusted deposition[d]	–9.4%	+7.1%
S4	Decreased fossil fuel burning emissions	–81.3%	+7.1%
S5	Increased photochemical removal	+60.1%	+7.1%

[a] This is the observed relative change in the corresponding budget term compared to scenario S1; see Table 3.
[b] These changes are calculated relative to scenario S1.
[c] This is the change caused by using ERA-Interim data instead of operational data.
[d] In order to reduce the interhemispheric gradient observed in S3a, the original soil deposition velocities reported by *Sanderson et al.* [2003] above forests and Savannah ecosystem types were increased by 10%, and the deposition velocities to agricultural regions were decreased by 10%. As a result, the SH H_2 mixing ratios decrease, whereas the NH mixing ratios remain more or less the same.

well known [*Sander et al.* 2006]. Furthermore, the chemical lifetime of 8.6 years for the reaction of CH_4 with OH is adequately reproduced by the TM5 model. This indicates that the modeled mixing ratios of OH are realistic as well.

[18] Decreasing the photochemical production of H_2 is not considered because the source magnitude is in line with expectation for scenario S1. A reduction of the photochemical source magnitude by the required amount to close the H_2 budget will lead to an overall photochemical source strength for H_2 that is incompatible with the atmospheric budget of CO [*Ehhalt and Rohrer*, 2009]. Other separate scenarios, i.e., reducing the H_2 emissions due to N_2 fixation, would require changes that are outside the established error margins for these sources.

2.8. Quantifying the Agreement Between the Model Results and Observations

[19] In all comparisons discussed in the next sections, the agreement between the model results and the measurements is quantitatively analyzed by using the chi-squared value (χ^2) as a metric [*Meirink et al.*, 2008b; *Villani et al.*, 2010], calculated as follows:

$$\chi^2 \equiv \sum_{i=1}^{n} \frac{(x_i - y_i)^2}{\sigma_i^2}, \tag{6}$$

where $i \in [1, n]$ is the index of measurement i with a value of y_i approximated by the model value x_i for a set of n measurements. The square of the standard deviation σ_i is calculated by the following:

$$\sigma_i^2 \equiv \sigma_{x,i}^2 + \sigma_{y,i}^2. \tag{7}$$

The uncertainty in the observations $\sigma_{y,i}$ is calculated using the following expression:

$$\sigma_{y,i}^2 \equiv \sigma_{\text{meas},i}^2 + \sigma_{y,\text{time},i}^2. \tag{8}$$

The measurement uncertainty $\sigma_{\text{meas},i}$ is estimated at 2% for the measured H_2 mixing ratios and at 5‰ for the measured isotopic compositions. In the case that time averaging is used to calculate a measured value y_i, the standard deviation $\sigma_{y,\text{time},i}$ over the time averaging period is calculated. The uncertainty in the model results $\sigma_{x,i}$ is calculated by the following:

$$\sigma_{x,i}^2 \equiv \sigma_{\text{trans},i}^2 + \sigma_{\text{sub},i}^2 + \sigma_{x,\text{time},i}^2. \tag{9}$$

Here, the uncertainty due to errors in atmospheric transport $\sigma_{\text{trans},i}$ is estimated by calculating the standard deviation over a model value x_i obtained by three different interpolation methods [*Bergamaschi et al.*, 2005]. The uncertainty due to subgrid variability in processes such as the emissions and planetary boundary layer (PBL) height ($\sigma_{\text{sub},i}$) is estimated at 2% for the H_2 mixing ratios calculated for background stations, and at 5% for continental stations. For $\delta D[H_2]$, we adopt $\sigma_{\text{sub},i} = 11‰$ because only a small fraction ($\approx$10%) of the uncertainties in the H_2 and HD mixing ratios is not correlated. For example, H_2 and HD are both emitted as a result of biomass burning. Because the isotope signature is a fixed value, a fixed ratio exists between the emitted amounts of H_2 and HD. Therefore, only the uncertainty in the isotope signature propagates into the uncertainty in the modeled isotopic composition. In the case that time averaging is used to calculate a modeled value x_i, the standard deviation $\sigma_{x,\text{time},i}$ of the model values is calculated over the time averaging period.

[20] Because the number of observations determine the overall value of χ^2, it is useful to scale it by the number of degrees of freedom ($\nu = n - 1$) which yields the reduced chi-squared value:

$$\tilde{\chi}^2 \equiv \frac{\chi^2}{\nu}. \tag{10}$$

This way, the goodness of fit of model results to different data sets can be compared using a normalized statistical value. Generally, a value of $\tilde{\chi}^2$ that is much larger than unity indicates poor agreement between the model results and the measurement data.

[21] The above-mentioned uncertainties that are used to calculate the $\tilde{\chi}^2$ values can also be used to calculate the uncertainties in the global budget. That is, a $\tilde{\chi}^2$ value around unity means that the model results and measurements agree within the ranges of uncertainty. Thus, the valid ranges for the magnitudes of the individual sources and sinks in the budget can be determined by applying perturbations in these magnitudes such that the ranges of uncertainty in the global burden or global mean isotopic composition are exceeded. Herein, the isotope signatures reported in *Pieterse et al.* [2011] are also used. Generally, the model uncertainties are larger than the uncertainties in the measurements (see above). Therefore, the values of 5% and 11‰ are adopted for the uncertainties in the global burden and global mean isotopic composition, respectively. The ranges obtained by the most stringent constraint (the measured global burden or the measured global mean isotopic composition) are then adopted as the ranges of uncertainty for each budget term.

3. Results

[22] In the following sections, the model results produced by the seven scenarios (see Table 1) are evaluated using available measurements. The analysis starts by comparing the modeled and measured seasonal variability in the H_2 mixing ratios for the EuroHydros and CSIRO stations. Section 3.2 evaluates the modeled latitudinal variability in $\delta D[H_2]$ using available measurements. Subsequently, the regional short-term variability in the EuroHydros H_2 measurements is investigated in section 3.3. The overall implications of this analysis for the global budget of H_2 are presented in section 4.

3.1. Seasonal Variability in H_2

[23] In Figure 1, the TM5 model results are compared to the measurements from the EuroHydros project. Table 2 lists the quantitative measure ($\tilde{\chi}^2$) for the agreement between the model results and the measurements. The reference scenario (S1, black dotted line) consistently underestimates the measured H_2 mixing ratios.

[24] In contrast, increasing the deposition resistance values for snow and water surfaces, wetted surfaces, vegetation leaf surfaces, and leaf mesophyll tissue (S2, black dashed line) leads to a large overestimation in the modeled H_2

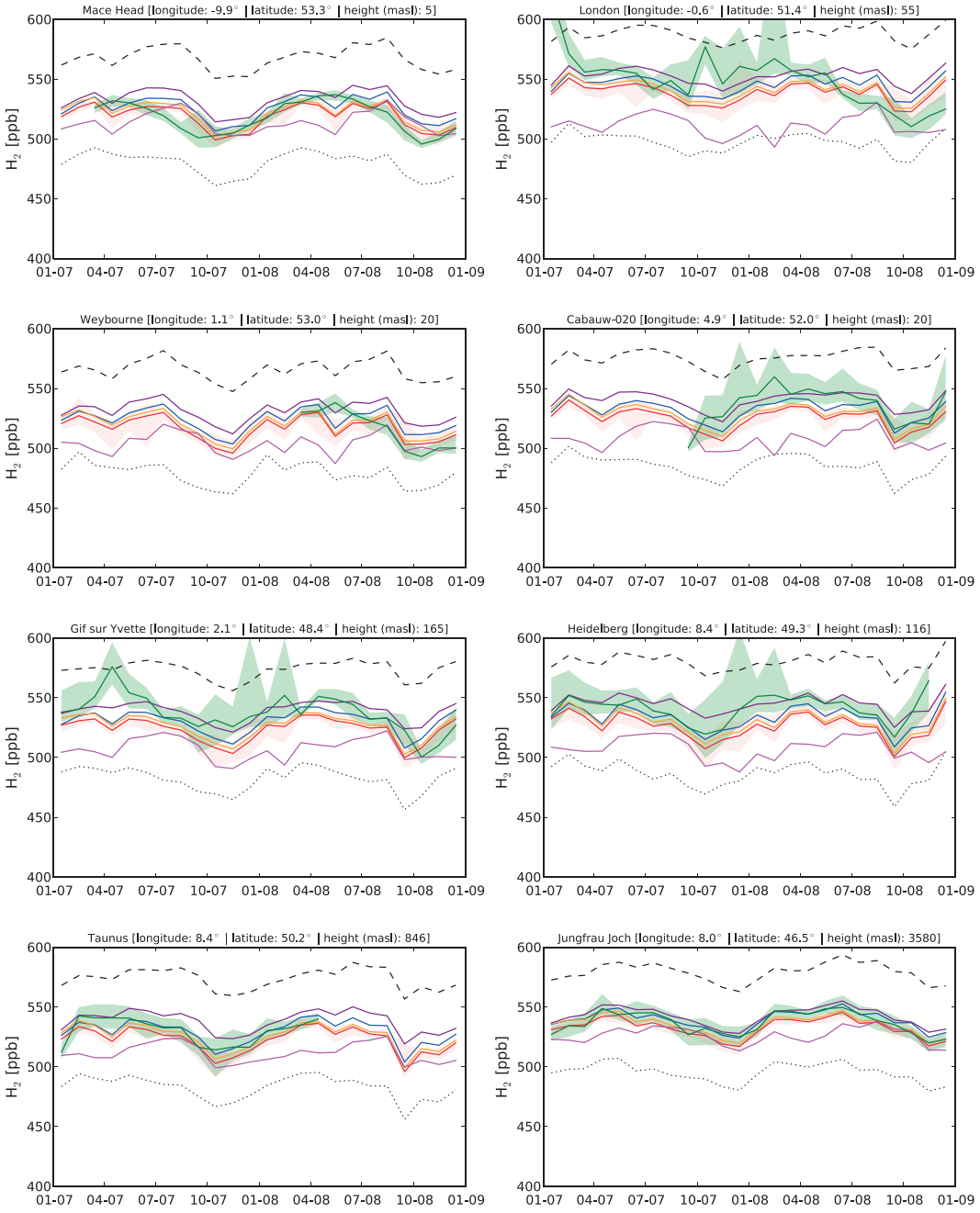

Figure 1. Comparison of modeled monthly median H_2 mixing ratios with available measurements from the EuroHydros project. The green lines represent the observational data. The following model scenarios are shown: S1 (dotted), S2 (dashed), S3a (blue), S3b (orange), S3c (red), S4 (magenta), and S5 (purple). The shaded areas indicate the lower and upper quartiles of the variability in the measurements (green) and model results for scenario S3c (red). Dates on the *x* axis are shown in MM-YY format.

mixing ratios. Thus, deposition is clearly underestimated in this scenario. Reducing the in-canopy deposition resistance (S3a, blue lines) leads to much better agreement with the observations, especially at the background stations (e.g., at Mace Head and Jungfraujoch). Remaining discrepancies between the model results and the nonbackground observations in Figure 1 (e.g., at Cabauw and London) can be attributed to the limited model resolution and are further explored in section 3.3. As expected, the lower in-canopy resistance combined with lower ocean H_2 emissions due to N_2 fixation (S3b, orange lines) has no significant effect for the European stations and leads to agreement between the model and the measurements similar to scenario S3a. This is also the case when the soil deposition velocities for forest and Savannah ecosystems are increased, whereas the velocities are decreased for agricultural regions (S3c red lines). Decreasing the fossil fuel emissions (S4, magenta lines) leads to a very poor model performance, especially

Table 2. Overview of $\tilde{\chi}^2$ Values[a] for Different Model Scenarios for H_2 and $\delta D[H_2]$

	Sampling Method	Parameter	n	$\tilde{\chi}^2$						
				S1	S2	S3a	S3b	S3c	S4	S5
Performance per comparison study										
Section 3.1, EuroHydros data	noontime[b]	H_2	10426	4.5	2.3	0.9	1.0	1.1	2.9	0.8
Section 3.1, CSIRO data	event	H_2	663	4.5	9.7	1.6	1.0	1.0	1.3	1.4
Section 3.2, Mean latitudinal gradient	[c]	$\delta D[H_2]$	48	1.5	0.4	0.4	0.8	0.4	1.7	4.3
Section 3.2, Seasonal latitudinal gradient	event	$\delta D[H_2]$	321	3.0	0.9	0.9	0.8	1.0	3.9	5.1
Section 3.2, Seasonal latitudinal gradient	event	H_2	382	6.8	12.1	1.7	1.2	1.1	1.5	2.3
Section 3.3, EuroHydros data	continuous	H_2	72026	5.9	4.7	1.1	1.1	1.2	3.7	1.2
Section 3.3, EuroHydros data (w/o London)	continuous	H_2	63392	6.4	4.7	1.0	1.0	1.1	3.5	1.0
Overall performance for H_2			83497	5.8	4.5	1.1	1.1	1.2	3.6	1.1
Overall performance for $\delta D[H_2]$			369	2.8	0.9	0.9	0.8	0.9	3.6	5.0

[a] See equation (10) in Section 2.4.

[b] The local noontime model results were sampled for this comparison; see section 2.4.

[c] Most measurement data were obtained during ship cruises on the Atlantic and Pacific Ocean. Furthermore, exact sampling times were not available for all data. Therefore, model data above the free Atlantic and Pacific Ocean (far away from the land masses) were selected to calculate an overall annual mean latitudinal gradient. Subsequently, the model values for the different stations were obtained by interpolation to the different station latitudes.

for London and the other low-altitude continental stations. Increasing the photochemical removal of H_2 by OH (S5, purple lines) improves the agreement between the model and measurements.

[25] These findings are confirmed by the $\tilde{\chi}^2$ values in the first row of Table 2. $\tilde{\chi}^2$ values around 1 for all three scenarios S3a, S3b, and S3c indicate that the performed changes in the deposition parametrization lead to model results that agree well with the EuroHydros observations. The large $\tilde{\chi}^2$ value of 2.9 obtained for scenario S4 confirms that reducing the fossil fuel emissions does not lead to a better model performance. A $\tilde{\chi}^2$ value around 1 for scenario S5 confirms that increasing the photochemical removal of H_2 also leads to a better agreement between the model results and the EuroHydros observations.

[26] The comparison of the scenario results with the independent data provided by CSIRO in Figure 2 show that scenario S3a (blue lines) slightly overestimates the H_2 mixing ratios for the stations on or near Antarctica. This suggests that either too much H_2 is emitted or too little H_2 is removed in the SH. One budget term that can offset these high southern latitude H_2 levels are the H_2 emissions from the oceans. Indeed, reducing the H_2 emissions due to nitrogen fixation to the oceans (S3b) shows a slight improvement in the agreement between the model results and observations. This improvement indicates that the emission source strength of 5 Tg H_2/yr due to N_2 fixation in the oceans might be too large, possibly only for the Arctic and Antarctic regions, as suggested earlier by *Herr et al*. [1981, 1984]. Alternatively, the overestimation could be caused by the larger vegetation resistances in the corrected deposition scheme resulting in much lower deposition velocities calculated for the rainforest and Savannah ecosystems than calculated in *Pieterse et al.* [2011]. Indeed, the agreement also improves by increasing the deposition velocities for the forest and Savannah ecosystem types (S3c). The results obtained with scenarios S4 and S5 are slightly worse than the results obtained with scenarios S3a–S3c, which is reflected by the larger $\tilde{\chi}^2$ values (1.3 and 1.4, respectively) in the second row of Table 2. Overall, scenarios S3b and S3c lead to the best agreement ($\tilde{\chi}^2$=1.0).

[27] Just as in our previous study [*Pieterse et al.*, 2011], the model does not capture the seasonal cycle at Alert well because it assumes that little or no deposition will occur in (partly) snow-covered regions. Hence, deposition starts affecting the modeled H_2 mixing ratios 3 months later in the season than observed in the measurements. The measurements at Mauna Loa show more variability than captured by the model because of the very coarse model resolution (6 by 4 degrees) at that location. As the largest part of the surface of the corresponding grid cell lies above the Pacific Ocean, the model might not capture the potential effect of local emissions from Hawaii on the measured H_2 mixing ratios.

3.2. Latitudinal Variability in δD[H_2]

[28] Figure 3 shows the modeled latitudinal gradient in $\delta D[H_2]$, sampled at the oceanic meridians, compared to available measurement data.

[29] The results of scenarios S2–S3c are in much better agreement with the observations than scenario S1. This is partly caused by the new stratospheric parametrization. Depending on the CH_4 mixing ratio, the parametrized stratospheric values for $\delta D[H_2]$ are >10‰ larger in this work than the values obtained with the parametrization used in *Pieterse et al.* [2011]. The actual corrections imposed by the new stratospheric parametrization are discussed in section 4. The $\tilde{\chi}^2$ values for the isotope results are shown in the third row of Table 2. Because the uncertainty in the measurement data is large, it is not possible to make a statistically sound distinction between scenarios S2–S3c. It is however obvious that scenarios S4 and S5 do not agree with the measurements, especially for the NH.

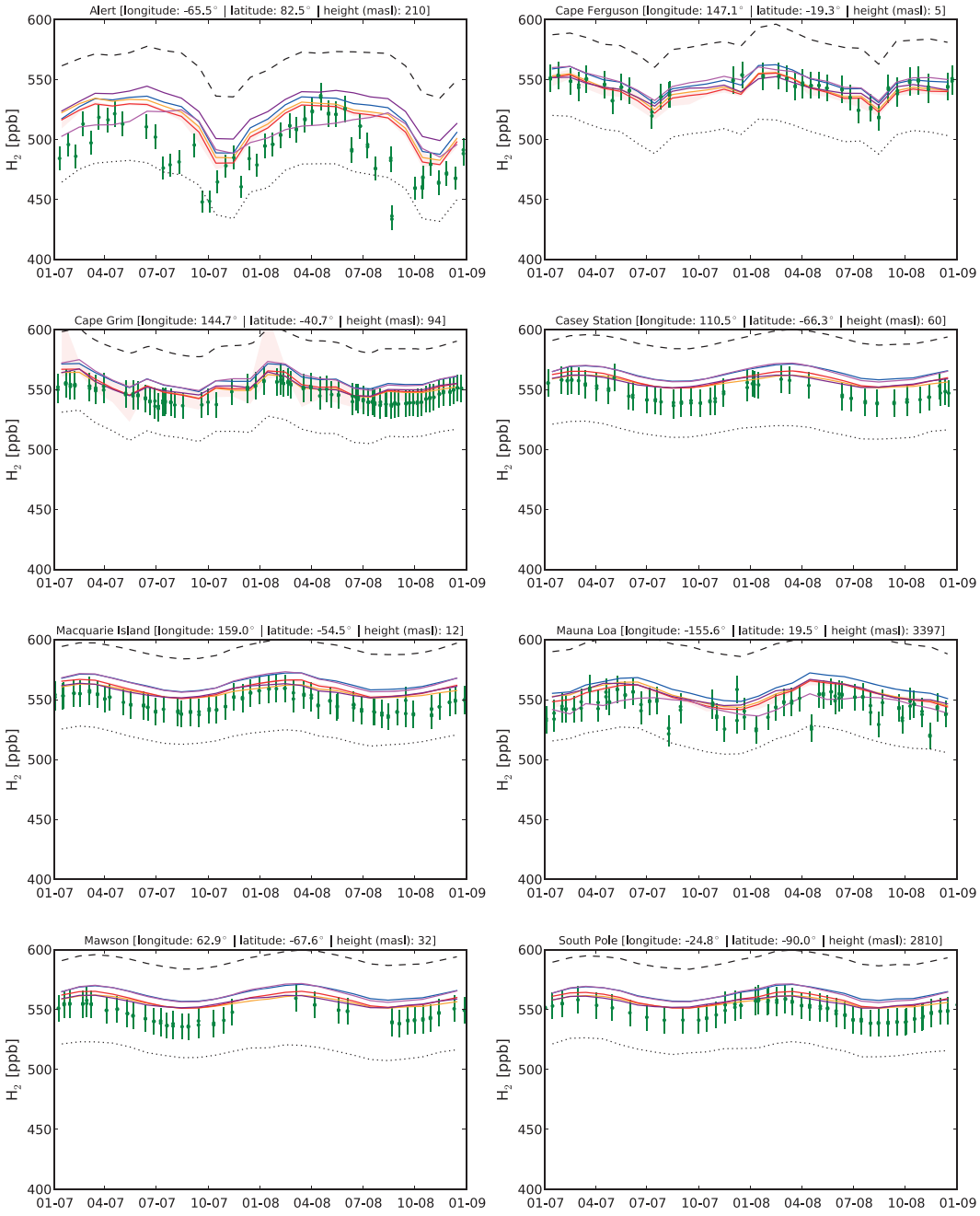

Figure 2. Comparison of modeled monthly median H_2 mixing ratios with available measurements from the CSIRO flask sampling network. The circles represent the event samples. The following model scenarios are shown: S1 (dotted), S2 (dashed), S3a (blue), S3b (orange), S3c (red), S4 (magenta), and S5 (purple). The shaded areas indicate the lower and upper quartiles of the variability in the model results for scenario S3c (red). Dates on the *x* axis are shown in MM-YY format.

[30] A more quantitative comparison among scenarios S2–S3c can be found in the seasonal evolution of the modeled latitudinal gradient of $\delta D[H_2]$ and H_2 mixing ratios measured at five stations (Alert, Mace Head, Cape Verde, Amsterdam Island, and the South Pole) in the EuroHydros project [*Batenburg et al.*, 2011], averaged for the years 2007 and 2008 (see Figure 4). Again, it is clear that scenarios S4 and S5 do not lead to realistic values for $\delta D[H_2]$ and are therefore not further discussed here. The $\tilde{\chi}^2$ values for the goodness of fit of the isotopic compositions in the fourth row of Table 2 show that scenarios S2–S3c are in good agreement with the observed mean latitudinal gradient of $\delta D[H_2]$. At the same time, the $\tilde{\chi}^2$ values for the accompanying H_2 mixing ratios shown in the fifth row of Table 2 are poor for scenarios S2 and S3a. Thus, scenarios S3b and S3c show the best performance for the H_2 mixing ratios and isotopic compositions that were measured simultaneously at the EuroHydros stations.

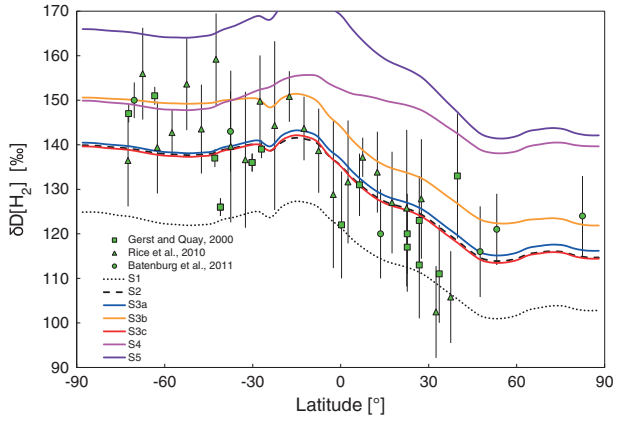

Figure 3. Comparison of the modeled free oceanic latitudinal gradient of $\delta D[H_2]$ with available measurement data. The green squares represent data points from *Gerst and Quay* [2000], the green triangles represent data points from *Rice et al.* [2010], and the green circles represent data points from the EuroHydros project [*Batenburg et al.*, 2011]. The following model scenarios are shown: S1 (dotted), S2 (dashed), S3a (blue), S3b (orange), S3c (red), S4 (magenta), and S5 (purple). Scenarios S2–S5 use the updated stratospheric parametrization derived from the CARIBIC measurements [*Batenburg et al.*, 2012] as upper-boundary condition.

[31] The seasonal mean values assigned to the highest NH latitude are obtained using measurements from Alert. Here, the discrepancy between the results of both model scenarios and the observed seasonal cycle is again attributed to the fact that in TM5, it is assumed that deposition in the snow-covered regions does not occur (see section 3.1).

[32] Another clear feature is the consistent negative bias of scenarios S2, S3a, and S3c relative to the observed isotopic composition at the highest SH latitudes (also visible in Figure 3). The agreement is improved for scenario S3b, but it appears that reducing the global emission source strength for H_2 due to N_2 fixation processes in the oceans leads to too large values for $\delta D[H_2]$ at the mid-latitude stations. Possibly, these emissions are only overestimated for the Arctic and Antarctic regions [*Herr et al.*, 1981] and [*Herr*, 1984].

The larger values for the isotopic composition might also be explained by the exchange of tropospheric air with stratospheric air that is much more enriched in HD in the Antarctic region than at the lower SH latitudes. The modeled isotopic composition from 30°S to 90°S is very sensitive to the isotopic composition that is assumed for the stratosphere from 60°S to 90°S [*Pieterse et al.*, 2011]. For this region, a negative bias of 10‰ between the modeled surface values and observations, as shown in Figure 4, can be explained by underestimating the isotopic composition in the stratosphere by 20‰. Possibly, this is related to the CH_4 background values that are used to calculate the stratospheric boundary condition. At latitudes above 60°S, these fields show CH_4 mixing ratios at the tropopause that are up to 25% lower than for instance a climatology obtained from the Halogen Occultation Experiment [*Grooß and Russell III*, 2005]. This can be the result of model transport errors in the STE [*Noije et al.*, 2004; *Pieterse et al.*, 2011]. In view of equation (1), these discrepancies could easily explain why the SH isotopic compositions are underestimated by the current TM5 model setup. As the differences between the modeled and observed H_2 mixing ratios are small, it is not expected that this discrepancy is of large importance for closing the global H_2 budget.

3.3. Regional Scale Variability in H_2 Over Europe

[33] Figure 5 shows the aggregated hourly average H_2 mixing ratios as a function of ECMWF surface wind direction for the eight EuroHydros stations where continuous measurements were performed. The median, upper quartile, 95th percentile, lower quartile, and 5th percentile were calculated over all values attributed to each wind sector. The median is shown as the white horizontal line in each colored bar that is bound by the lower and upper quartile. The 5th and 95th percentiles are shown as whisker lines. Scenarios S1, S2, S3a, S4, and S5 are not shown in the figure because their overall performance for the EuroHydros stations was poorer than for scenarios S3b and S3c (see section 3.1). Because scenarios S3b and S3c showed a similar performance, only the results of scenario S3c are shown here for clarity.

[34] The modeled values for this scenario show a good correspondence with the measurements, with the exception of specific wind directions, e.g., the east to southeast wind sector for the station at Cabauw. To further investigate the causes for these discrepancies, the differences between the modeled and the observed median H_2 mixing ratios are shown as colored wind roses in a map plot in Figure 6.

[35] At Mace Head [*Grant et al.*, 2010], the modeled median H_2 mixing ratios corresponding to the marine sector (south to northwest) agree well with the measurement data, whereas the model underestimates the observations in the land sector. This indicates again that either deposition is overestimated or that the surface emissions are underestimated. The results for the station in Egham located west to southwest of London are clearly affected by the fact that the model grid cell containing this station also contains a highly populated urban area (and the associated emissions), whereas the station itself is located in a rural area West of the London city center. As a result, the measurements affected by the emissions from London city (Easterly wind sector) are relatively well captured by the model, whereas the model results from the other wind directions overestimate the measured H_2 mixing ratios.

[36] The measurements performed at the tall tower station near Cabauw in The Netherlands are strongly influenced by urban activity [*Popa et al.*, 2011]. Contrary to the station near London, the station at Cabauw is located in a grid cell with much less urban influence than representative for this site. In reality, the measurements are severely influenced by emissions originating from the urban and industrial areas in Utrecht (The Netherlands), the Ruhr area (Germany), and Antwerp (Belgium), from the northern to southwesterly wind directions, respectively. Hence, the model results in the marine sector (West to North) are in closest agreement with the observations, while the measurements are underestimated for other wind directions.

[37] For similar reasons, the measurements at Gif-sur-Yvette are underestimated in the wind sector where the station is influenced by the city of Paris (north to northeast).

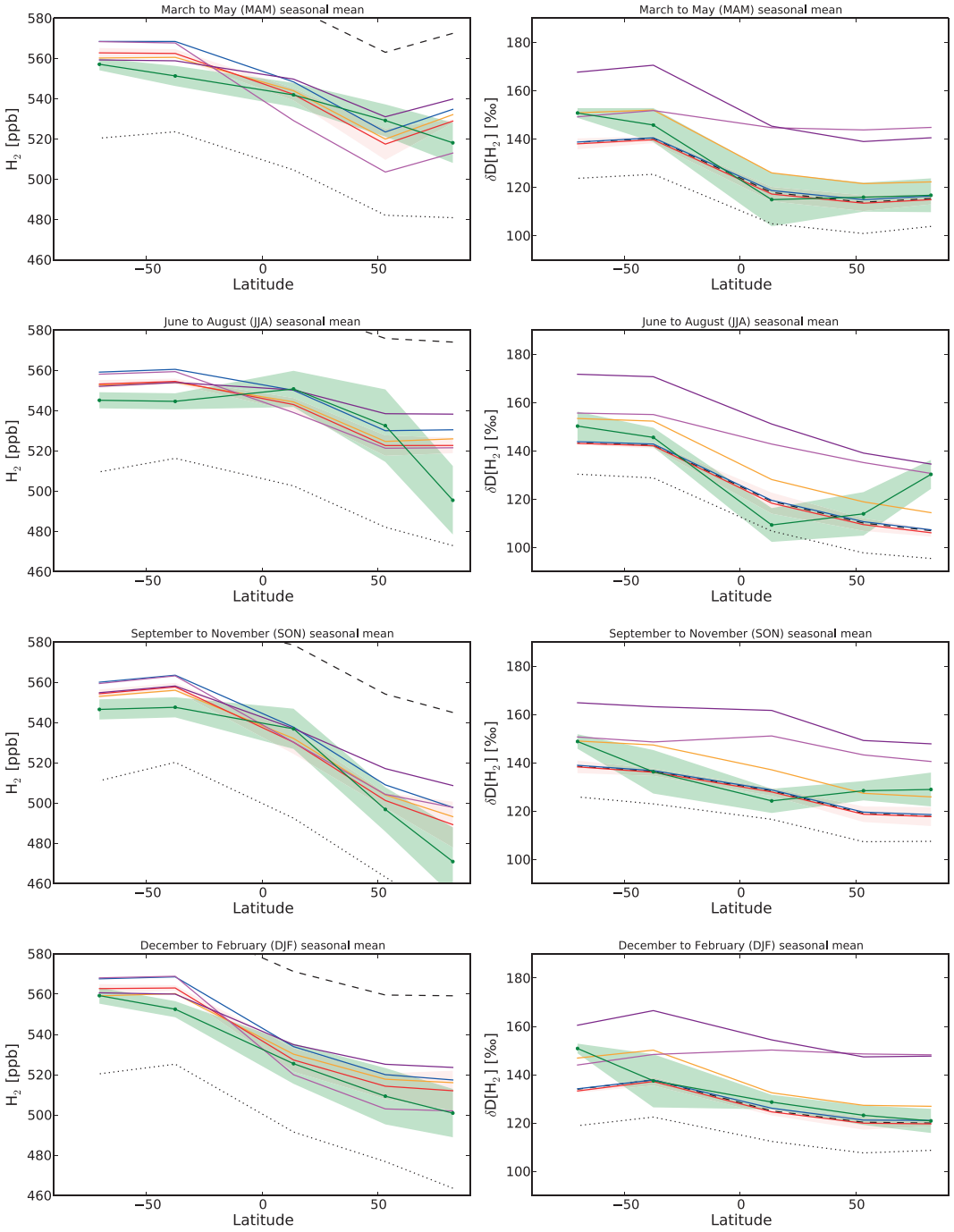

Figure 4. Comparison of the modeled seasonal mean latitudinal gradients of the H_2 mixing ratio (left) and isotopic composition (right) with available measurement data (green) from the EuroHydros project [*Batenburg et al.*, 2011]. The shaded areas indicate the within-season standard deviations of the measurements (green) and model results for scenario S3c (red). The following model scenarios are shown: S1 (dotted), S2 (dashed), S3a (blue), S3b (orange), S3c (red), S4 (magenta), and S5 (purple). Scenarios S2–S5 use the updated stratospheric parametrization derived from the CARIBIC measurements [*Batenburg et al.*, 2012] as upper-boundary condition.

At Weybourne (United Kingdom), the signals arriving from the urban area of Norwich, southeast of the station, are adequately captured by the model. For the Southern to Western wind directions, the model overestimates the H_2 mixing ratios because the emissions in the grid cell containing the Weybourne station are larger than representative for these wind directions. Similarly, deposition is overestimated for the Northern to Eastern wind directions.

[38] In Heidelberg and Taunus (Germany), the model results are generally in good agreement with the observations, as is the case for the observations at the Jungfraujoch in Switzerland [*Bond et al.*, 2011]. For the station located

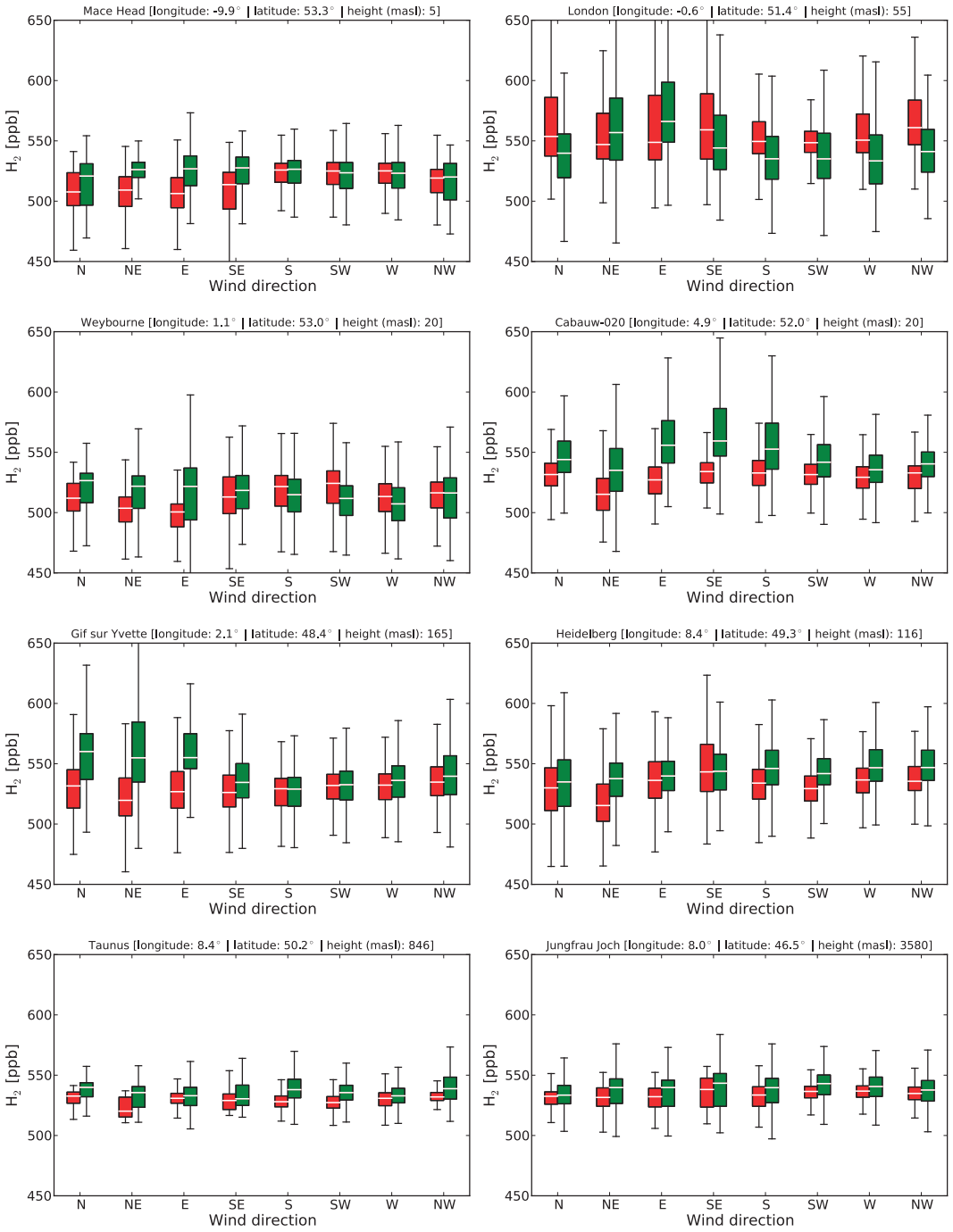

Figure 5. Comparison of modeled H_2 mixing ratios obtained with scenario S3c (red) with available measurement data (green) from the EuroHydros project, aggregated per wind sector. The median values are shown as white horizontal lines in the boxes that show the upper and lower quartiles. The 5 and 95 percentiles are indicated by the whiskers.

northWest of Bialystok (Poland), the model underestimates the measured H_2 mixing ratios arriving from the city nearby the tower. The H_2 mixing ratios in air masses arriving from the east and northeast are also underestimated, which means that the deposition of H_2 to the large evergreen forest and arable regions in the direct vicinity east and northeast of the station is overestimated.

[39] The $\tilde{\chi}^2$ values in the sixth row of Table 2 confirm that scenarios S3b and S3c show the best overall agreement with the continuous observations from the EuroHydros project. Scenario S5 is not considered here because of its poor performance for the comparisons in the previous sections. More detailed analysis on the main contributors to the overall $\tilde{\chi}^2$ values revealed that none of the model scenarios produces realistic values for the station at Egham. Indeed, removing the data from this station results in $\tilde{\chi}^2$ values closer to unity; see seventh row in Table 2. The remaining discrepancies between the model results and the measurement data can

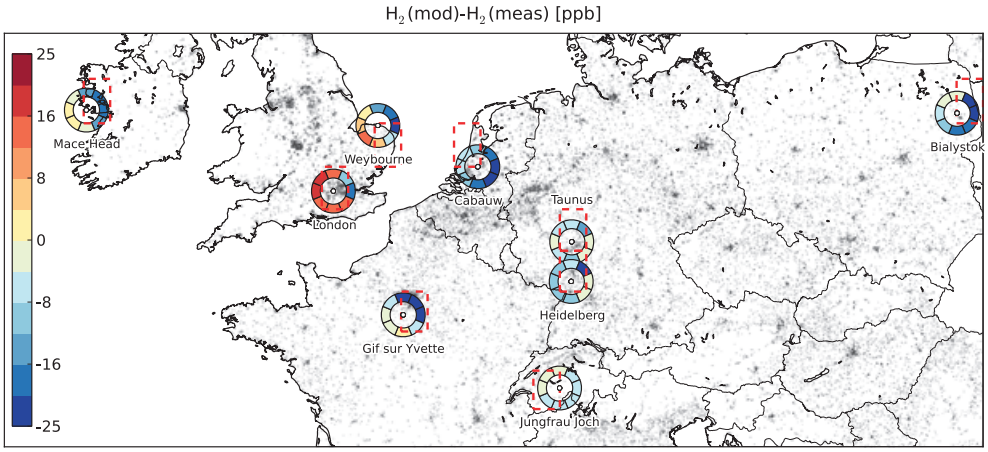

Figure 6. Overview of the difference between the modeled and measured H_2 median mixing ratios of scenario S3c, calculated per wind sector and shown as a colored wind rose around the location of each station (white circle). Urban areas shown in gray were obtained from the Corine Land Cover (CLC) 2006 database [*EEA*, 2007]. The 1 by 1° grid cells that belong to each station are shown as dashed red squares.

in general be attributed to the limited representativeness of the relatively coarsely gridded model surface emissions and deposition mass fluxes for capturing certain station-specific local influences. Such representation errors were also found in integrated model studies investigating other species, for example carbon dioxide [*Patra et al.* 2008].

4. Implications for the Global Budget

[40] Table 3 shows the global budgets for the year 2008 of all seven scenarios, along with a selection of previously derived budgets. The atmospheric burden of 165 Tg H_2 associated with the scenarios that agree best with the observations, i.e., scenarios S3b and S3c, is significantly larger than the burden for the reference scenario (S1, 154 Tg H_2). This increase of 7.1% is larger than corrections related to the calibration scale revision (see section 2.4) and requires further explanation. Due to slower vertical mixing associated with the use of ERA-Interim data, steeper near-surface gradients are obtained because the calculated PBL heights are on average 10% smaller. This leads to near-surface mixing ratios that are larger compared to the free tropospheric mixing ratios and, as a consequence, to stronger removal of H_2 by deposition compared to the previous model setup (see Table 3). Therefore, the modeled tropospheric burden is smaller for scenario S1.

[41] The difference between the results of scenarios S1 and S2 shows the impact of using larger resistance values ($1 \cdot 10^9$ sm^{-1}) for the deposition of H_2 to snow and water surfaces, wetted surfaces, vegetation leaf surfaces, and leaf mesophyll tissue. Clearly, the values for the tropospheric burden and atmospheric lifetime (176 Tg H_2 and 2.6 years) obtained with scenario S2 are too large. At the same time, the correction required for the stratospheric isotopic compositions of –137‰ also shows that values obtained for $\delta D[H_2]$ in the stratosphere are unrealistic. Reducing the in-canopy resistance term (scenario S3a) drastically improves the overall model performance. The results in the previous sections showed that the remaining gap of 2 Tg H_2 between scenario S3a and scenario S3b or S3c is likely caused by either too little removal or too large emissions in the SH; reducing the H_2 emissions due to N_2 fixation in the oceans (scenario S3b) further improves the model performance. The approach of decreasing the soil deposition resistances for forest and Savannah ecosystem types (scenario S3c) leads to a comparable improvement. Alternatively, decreasing the biomass burning emissions could improve the agreement between the model and the observations of H_2. This would probably also increase the isotopic compositions in the SH, leading to a better agreement with the observations of $\delta D[H_2]$, as was the case for scenario S3b.

[42] Overall, the updated stratospheric parametrization imposes a smaller correction on the results produced by the stratospheric H_2 chemistry scheme in scenarios S3a–S3c than the previous version implemented in the reference scenario (around 1.0 instead of 2.4 Tg H_2). Also, the results produced by scenario S3c require no correction in the isotopic composition from the stratospheric parametrization. That is, scenario (S3c) driven by ERA-Interim data explains an important part of the observed variability in H_2 and $\delta D[H_2]$.

[43] The analysis in sections 3.1 and 3.2 showed that the agreement between the modeled H_2 mixing ratios and isotopic compositions and the observations from the Euro-Hydros network was very poor for scenario S4. Moreover, the resulting fossil fuel emission source magnitude of 3.2 Tg H_2/yr is outside the reported range of 5–25 Tg H_2/yr (see Table 3) and is therefore considered unrealistic. *Vollmer et al.* [2012] recently suggested a strong decrease in H_2 fossil fuel related emissions between 2000 and 2010. For the year 2005, they reported a value of 6.0 ± 1.5 Tg H_2/yr for the global emissions due to road transportation. Although the aggregated overall fossil fuel emissions in our study are much larger, the part assigned to road transportation is 6.9 Tg H_2/yr and therefore equal to the emissions estimated by *Vollmer et al.* [2012]. However, the emissions as a result of residential burning processes used in this study (9.0 Tg H_2/yr) are much larger than the value of 2.8 ± 0.7 Tg H_2/yr that was based on measurements performed

Table 3. Global Budget of H_2 for the Year 2008 Compared to Existing Budgets (Numbers in Tg H_2/yr)

	Novelli et al. [1999]	*Rhee et al.* [2006]	*Xiao et al.* [2007]	*Ehhalt and Rohrer* [2009]	*Pieterse et al.* [2011]	Scenarios in This Work						
						S1	S2	S3a	S3b	S3c	S4	S5
Sources												
Fossil fuel	15 ± 10	15 ± 6	15 ± 10	11 ± 4	17.0	17.1	17.1	17.1	17.1	17.1	3.2	17.1
Biomass burning	16 ± 5	16 ± 3	13 ± 3	15 ± 6	15.0	15.0	15.0	15.0	15.0	15.0	15.0	15.0
Ocean N_2 fixation	3 ± 2	6 ± 5		6 ± 3	5.0	5.0	5.0	5.0	3.0	5.0	5.0	5.0
Land N_2 fixation	3 ± 1	6 ± 5		3 ± 2	3.0	3.0	3.0	3.0	3.0	3.0	3.0	3.0
Photochemical production	40 ± 16	64 ± 12	77 ± 10	41 ± 11	37.3	36.9	36.8	36.9	36.9	36.9	36.9	36.4
Vertical flux[a]					-0.1	0.3	-0.3	0.0	0.1	0.1	0.1	0.1
Stratospheric correction flux[b]					0.4	2.4	-7.5	-2.1	-1.2	-1.1	-0.9	-1.1
Total	77 ± 16	107 ± 15	105 ± 10	76 ± 14	77.6	79.7	69.1	74.9	73.9	76.0	62.3	75.5
Sinks												
Photochemical removal	19 ± 5	19 ± 3	18 ± 3	19 ± 5	22.1	21.3	24.5	23.1	22.8	22.8	22.8	34.1
Deposition	56 ± 41	88 ± 11	85 ± 5	60^{+30}_{-20}	55.8	58.4	44.0	51.4	50.9	52.9	39.5	41.2
Total	75 ± 41	107 ± 11	105[c]	79^{+30}_{-20}	77.9	79.7	68.5	74.5	73.7	75.7	62.3	75.3
Overall												
Tropospheric burden (Tg H_2)	155 ± 10	150[d]	149 ± 23	155[e] ±10	157[f]	154[f]	176[f]	167[f]	165[f]	165[f]	165[f]	165[f]
Tropospheric lifetime (yr)	2.1	1.4	1.4	2.0	2.0[f]	1.9[f]	2.6[f]	2.3[f]	2.2[f]	2.2[f]	2.7[f]	2.2[f]
Isotopic composition (‰)[g]					128	128	144	139	144	139	155	167
Stratospheric correction (‰)[g]					29	59	-137	-22	-16	0	-32	-53

[a]This term accounts for the influx of H_2 from the stratospheric model levels below 100 hPa.
[b]This term accounts for the stratospheric correction (see section 2.5) for the part of the stratosphere that is in the model domain down to 100 hPa.
[c]Includes export to stratosphere of 1.9 Tg H_2 per year.
[d]Calculated from sources and lifetime.
[e]From *Novelli et al.* [1999].
[f]The values in the table are calculated from the burden and lifetimes of H_2 in the model domain from the surface down to 100 hPa by assuming that 92.3% of the mass in this domain resides in the troposphere.
[g]The stratospheric correction is part of the overall value for the isotopic composition relative to VSMOW down to 100 hPa.

in Switzerland. A possible explanation for the discrepancy between our results and those by *Vollmer et al.* [2012] may be that the latter are not representative for the entire domain of the EuroHydros observations and that H_2 emissions from natural gas may be significantly larger.

[44] It is also not likely that the global budget can be closed by increasing the photochemical removal (scenario S5). In order to obtain the required increase of 9.5 Tg H_2/yr in the photochemical removal of H_2, the rate coefficients of the reactions of H_2 and HD with OH had to be increased by 53%. This perturbation is outside the range of uncertainty of ±10% reported by *Sander et al.* [2006]. Furthermore, the resulting overall sink of 34.1 Tg H_2/yr is outside the range of 14–24 Tg H_2/yr reported in earlier studies; see Table 3.

[45] A scenario to investigate the impact of reducing the photochemical source to 23 Tg H_2/yr was not considered because this approach would imply an unrealistically low photochemical source for CO from formaldehyde. H_2 and CO are both photochemically produced from formaldehyde, and therefore, the photochemical source magnitudes of both species are intertwined [*Sander et al.* 2006]. Contrary to H_2, the photochemical source magnitude of CO is well constrained because deposition plays only a minor role in the removal of CO from the atmosphere [*Houghton et al.*, 2001]. In this TM5 model setup, 1.24 Pg CO/yr is produced from formaldehyde, which is in good agreement with the photochemical source magnitudes of 1.24 and 1.29 Pg CO/yr reported by [*Houghton et al.*, 2001] and [*Kopacz et al.* 2010], respectively. In all, the TM5 chemistry scheme produces 34 Tg CO per Tg H_2 from formaldehyde, which also agrees well with the expected ratio of 36 Tg CO per Tg H_2 reported by *Ehhalt and Rohrer* [2009]. A reduction of the photochemical source strength for H_2 to the above-mentioned value would therefore yield a photo chemical source strength for CO between 0.78 and 0.83 Pg CO/yr. These values would be too small in view of the reported values.

[46] For similar reasons, *Ehhalt and Rohrer* [2009] have postulated that the budgets reported by *Rhee et al.* [2006] and *Xiao et al.* [2007] (see Table 3) might be compromised by an unrealistically large photochemical source of H_2 compared to what is expected from the photochemical source of CO. Using the ratio of 34 Tg CO per Tg H_2, the photochemical source magnitudes for H_2 of *Rhee et al.* [2006] and *Xiao et al.* [2007] in Table 3 imply photochemical source magnitudes of 2.17 and 2.61 Pg CO/yr, respectively. These magnitudes are a factor of 1.7 and 2.1 larger than the present-day estimates and indicate that a photochemical source magnitude of 37 Tg H_2/yr would have been more realistic. Because this analysis is performed by using a chemical reaction mechanism implemented in a full global CTM, these results form an independent confirmation of the conclusion by *Ehhalt and Rohrer* [2009] that the above-mentioned large estimates for the removal of H_2 by deposition should not be used for future studies.

[47] Since scenario S3c produces the most realistic values for the H_2 mixing ratios and requires little stratospheric forcing for the H_2 mixing ratios and isotopic compositions, deposition is identified as the most sensitive parameter to reestablish a closed global H_2 budget. Because of the high impact of deposition on the budget, the vertical transport in the model plays a very important role for H_2 in the troposphere. The magnitude of the deposition term in the budget shows a strong dependency on the vertical transport, indicating that H_2 and its isotopic signature put important constraints on atmospheric transport processes such as STE.

5. Conclusions

[48] We have further tested and updated the molecular hydrogen (H_2) isotope chemistry scheme in the two-way nested TM5 model [*Krol et al.*, 2005; *Pieterse et al.*, 2011]. In a first simulation (scenario S1) with the reference H_2 chemistry scheme, the atmospheric burden of H_2 was underestimated by 7.1%. This percentage is larger than the differences of 2.0–3.1% between the MPI-2009 scale and the old calibration scales. The additional gap is a consequence of using ERA-Interim meteorology for the model simulations described in this study. These data show more atmospheric stability resulting in increased values for the near-surface H_2 mixing ratios compared to the free tropospheric mixing ratios. As a result, the removal of H_2 by deposition increases, and the modeled atmospheric burden of H_2 decreases.

[49] During this research, we found out that the model setup in our previous study [*Pieterse et al.*, 2011] actually overestimated the H_2 deposition to snow, water, and vegetation surfaces. Avoiding deposition to these surfaces led to an overestimate of the tropospheric burden of 6.7% (S2) because of a too large in-canopy resistance term. We implemented a reduced in-canopy resistance, corresponding to canopy mixing times of 1–2 h, to describe the transport of H_2 through the canopy to the soil underneath. When the new description was in place, a good overall agreement between measurements and model results was obtained, except for an overestimate at high southern latitudes. This gap could be closed either by decreasing the H_2 emissions or by increasing deposition to the rainforest and savannah ecosystems by 2 Tg H_2/yr.

[50] Deposition is identified as the process to which the H_2 budget is most sensitive. Other processes, such as fossil fuel emissions and oxidation by OH, require much larger perturbations to close the H_2 budget. Thus, uncertainties in these parameters may play a role, but the required perturbations for single processes are often outside their established uncertainty ranges.

[51] All in all, scenario S3c produces the most realistic model results for H_2 and $\delta D[H_2]$, so it is adopted to update the global budget of H_2 previously reported in *Pieterse et al.* [2011]. The tropospheric burden is now estimated at 165 ± 8 Tg H_2, and the magnitudes of removal of H_2 by deposition and photochemical oxidation at 53 ± 4 and 23 ± 2 Tg H_2/yr, respectively. This results in a tropospheric lifetime of 2.2 ± 0.2 year. The photochemical production is estimated at 37 ± 4 Tg H_2/yr. It is therefore expected that the proposed budget provides a sufficiently accurate baseline scenario to evaluate the impact of increasing H_2 emissions on tropospheric chemistry and climate.

[52] **Acknowledgments.** This study was funded by the Dutch NWO-ACTS project 053.61.026 and the EuroHydros project, funded via the Sixth Framework Programme of the European Commission (SUSTDEV-2005-3.I.2.1 Atmospheric composition change: Methane, Nitrous Oxide

and Hydrogen). Further support was provided by the Pan-European Gas-AeroSOl-climate interaction Study (PEGASOS) funded by the European Commission under the Seventh Framework Programme (FP7-ENV-2010-265148). Andrew Rice from Portland State University (USA) and Paul Quay from the University of Washington (USA) are acknowledged for access to their H_2 isotope data. Finally, the Nederlandse Organisatie voor Wetenschappelijk Onderzoek (NWO) is acknowledged for providing the computational facilities to run the TM5 model.

References

Andreae, M. O., and P. Merlet (2001), Emission of trace gases and aerosols from biomass burning, *Global Biogeochem. Cycles*, *15*(4), 955–966, doi:110.1029/2000GB001382.

Batenburg, A. M., S. Walter, G. Pieterse, I. Levin, M. Schmidt, A. Jordan, S. Hammer, C. Yver, and T. Röckmann (2011), Temporal and spatial variability of the stable isotopic composition of atmospheric molecular hydrogen: Observations at six EUROHYDROS stations, *Atmos. Chem. Phys*, *11*, 6985–6999, doi:10.5194/acp–11–6985–2011.

Batenburg, A. M., T. J. Schuck, A. K. Baker, A. Zahn, C. A. M. Brenninkmeijer, and T. Röckmann (2012), The stable isotopic composition of molecular hydrogen in the tropopause region probed by the CARIBIC aircraft, *Atmos. Chem. Phys*, *12*(10), 4633–4646, doi:10.5194/acp-12-4633-2012.

Bergamaschi, P., M. Krol, F. Dentener, A. Vermeulen, F. Meinhardt, R. Graul, M. Ramonet, W. Peters, and E. J. Dlugokencky (2005), Inverse modelling of national and European CH_4 emissions using the atmospheric zoom model TM5, *Atmos. Chem. Phys*, *5*(9), 2431–2460, doi:10.5194/acp-5-2431-2005

Bond, S. W., M. K. Vollmer, M. Steinbacher, S. Henne, and S. Reimann (2011), Atmospheric molecular hydrogen (H_2): Observations at the high-altitude site Jungfraujoch, Switzerland, *Tellus B*, *63*(1), 64–76, doi:10.1111/j.1600–0889.2010.00509.x.

Bousquet, P., D. A. Hauglustaine, P. Peylin, C. Carouge, and P. Ciais (2005), Two decades of OH variability as inferred by an inversion of atmospheric transport and chemistry of methyl chloroform, *Atmos. Chem. Phys*, *5*(10), 2635–2656, doi:10.5194/acp–5–2635–2005.

Bousquet, P., et al. (2011), A three-dimensional synthesis inversion of the molecular hydrogen cycle: Sources and sinks budget and implications for the soil uptake, *J. Geophys. Res*, *116*, D01302, doi:10.1029/2010JD014599.

Brenninkmeijer, C. A. M., et al. (2007), Civil aircraft for the regular investigation of the atmosphere based on an instrumented container: The new CARIBIC system, *Atmos. Chem. Phys*, *7*(18), 4953–4976, doi:10.5194/acp–7–4953–2007.

Christian, T. J., B. Kleiss, R. J. Yokelson, R. Holzinger, P. J. Crutzen, W. M. Hao, B. H. Saharjo, and D. E. Ward (2003), Comprehensive laboratory measurements of biomass-burning emissions: 1. Emissions from Indonesian, African, and other fuels, *J. Geophys. Res*, *108*, 4719, doi:10.1029/2003JD003704.

Conrad, R., and W. Seiler (1985), Influence of temperature, moisture, and organic carbon on the flux of H_2 and CO between soil and atmosphere: Field studies in subtropical regions, *J. Geophys. Res*, *90*(D3), 5699–5709, doi:10.1029/JD090iD03p05699.

Dee, D. P., et al. (2011), The ERA-Interim reanalysis: Configuration and performance of the data assimilation system, *Quart. J. R. Meteorol. Soc*, *137*(656), 553–597, doi:10.1002/qj.828.

EEA, (2007), CLC2006 technical guidelines, *EEA Technical report No.17/2007*, European Environmental Agency.

Ehhalt, D. H., and F. Rohrer (2009), The tropospheric cycle of H_2: A critical review, *Tellus B*, *61*(3), 500, doi:10.1111/j.1600–0889.2009.00416.x.

Endresen, O., E. Sørgard, J. K. Sundet, S. B. Dalsøren, I. S. A. Isaksen, T. F. Berglen, and G. Gravir (2003), Emissions from international sea transport and environmental impact, *J. Geophys Res*, *108*(D17), 4560, doi:10.1029/2002JD002898.

Engel, A., and EUROHYDROS PIs, (2009), Eurohydros, a European network for atmospheric hydrogen observations and studies, *EUROHYDROS Final Report*, http://cordis.europa.eu/.

Erickson III, D. J., and J. A. Taylor (1992), 3-D tropospheric CO modeling—The possible influence of the ocean, *Geophys. Res. Lett*, *19*(19), 1955–1958, doi:10.1029/92GL01475.

Feck, T., J.-U. Grooß, and M. Riese (2008), Sensitivity of Arctic ozone loss to stratospheric H_2O, *Geophys. Res. Lett*, *35*, L01803, doi:10.1029/2007GL031334.

Feilberg, K. L., M. S. Johnson, and C. J. Nielsen (2004), Relative reaction rates of HCHO, HCDO, DCDO, $H^{13}CHO$, and $HCH^{18}O$ with OH, Cl, Br, and NO_3 radicals, *J. Phys. Chem. A*, *108*, 7393–7398, doi:10.1021/jp048329k.

Foken, T., et al. (2012), Coupling processes and exchange of energy and reactive and non-reactive trace gases at a forest site—results of the EGER experiment, *Atmos. Chem. Phys*, *12*(4), 1923–1950, doi:10.5194/acp–12–1923–2012.

Fowler, M., D. Lowry, R. Fisher, M. Lanoisellé, and E. Nisbet (2011), The long-term (1996–2010) London record of carbon monoxide and molecular hydrogen : Evidence for improved air quality, *Geophys. Res. Abstr*, *13*, 12064–12064

Francey, R. J., et al. (1996), Global atmospheric sampling laboratory (GASLAB): Supporting and extending the Cape Grim trace gas program, in *Baseline Atmospheric Program Australia 1993*, pp. 23–25, Bureau of Meteorology and CSIRO Division of Atmospheric Research, Melbourne.

Ganzeveld, L. N., and Lelieveld J. (1995), Dry deposition parameterization in a chemistry general circulation model and its influence on the distribution of reactive trace gases, *J. Geophys. Res*, *100*(D10), 20999–2012, doi:10.1029/95JD02266.

Ganzeveld, L. N., J. Lelieveld, and G.-J. Roelofs (1998), A dry deposition parameterization for sulfur oxides in a chemistry and general circulation model, *J. Geophys Res*, *105*(D5), 5679–5694, doi:10.1029/97JD03077.

Ganzeveld, L. N., F. J. Dentener, J. Lelieveld, M. C. Krol, and G.-J. Roelofs (2002), Atmosphere-biosphere trace gas exchanges simulated with a single-column model, *J. Geophys Res*, *107*(D16), 4297–4317, doi:10.1029/2001JD000684.

Gerst, S., and P. Quay (2000), The deuterium content of atmospheric molecular hydrogen: Method and initial measurements, *J. Geophys. Res*, *105*(D21), 26433–26445, doi:10.1029/2000JD900387.

Gerst, S., and P. Quay (2001), Deuterium component of the global molecular hydrogen cycle, *J. Geophys. Res*, *106*, 5021–5031, doi:10.1029/2000JD900593.

Gery, M. W., G. Z. Whitten, J. P. Killus, and M. C. Dodge, (1988), Development and testing of the CBM-4 for urban and regional modelling, *Technical Report Rep. EPA-600/3-88-012*, U.S. Environ. Prot. Agency, Research Triangle Park, N.C.

Gery, M. W., G. Z. Whitten, J. P. Killus, and M. C. Dodge (1989), A photochemical kinetics mechanism for urban and regional scale computer modeling, *J. Geophys. Res*, *94*(D10), 12925–12956, doi:10.1029/JD094iD10p12925.

Grant, A., C. S. Witham, P. G. Simmonds, A. J. Manning, and S. O'Doherty (2010), A 15 year record of high-frequency, in situ measurements of hydrogen at Mace Head, Ireland, *Atmos. Chem. Phys*, *10*(3), 1203–1214, doi:10.5194/acp–10–1203–2010.

Grooß, J.-U., and J. M. Russell III (2005), Technical note: A stratospheric climatology for O_3, H_2O, CH_4, NO_x, HCl and HF derived from HALOE measurements, *Atmos. Chem. Phys*, *5*(10), 2797–2807, doi:10.5194/acp–5–2797–2005.

Hammer, S., and I. Levin (2009), Seasonal variation of the molecular hydrogen uptake by soils inferred from continuous atmospheric observations in Heidelberg, southwest Germany, *Tellus B*, *61*, 556–565, doi:10.1111/j.1600–0889.2009.00417.x.

Hauglustaine, D. A., and D. H. Ehhalt (2002), A three-dimensional model of molecular hydrogen in the troposphere, *J. Geophys. Res*, *107*(D17), 4330, doi:10.1029/2001JD001156.

Herr, F. L., M. I. Scranton, and W. R. Barger (1981), Dissolved hydrogen in the Norwegian Sea: Mesoscale surface variability and deep-water distribution, *Deep-Sea Res*, *28*(9), 1001–1016, doi:10.1016/0198-0149(81)90014-5.

Herr, F. L. (1984), Dissolved hydrogen in Eurasian Arctic waters, *Tellus B*, *36*(1), 55–66, doi:10.1111/j.1600-0889.1984.tb00052.x.

Houghton, J. T., Y. Ding, D. J. Griggs, M. Noguer, P. J. van der Linden, X. Dai, K. Maskell, and C. A. Johnson (2001), *Climate Change 2001: The Scientific Basis. Contribution of Working Group I to the Third Assessment Report of the Intergovernmental Panel on Climate Change*, chapter 4: Atmospheric Chemistry and Greenhouse Gases, Cambridge University Press, Cambridge, United Kingdom and New York, NY, USA.

Houweling, S., F. Dentener, and J. Lelieveld (1998), The impact of non-methane hydrocarbon compounds on tropospheric photochemistry, *J. Geophys. Res*, *103*(D9), 10673–10696, doi:10.1029/97JD03582.

Jordan, A., and B. Steinberg (2011), Calibration of atmospheric hydrogen measurements, *Atmos. Meas. Tech*, *4*(3), 509–521, doi:10.5194/amt–4–509–2011.

Kopacz, M., et al. (2010), Global estimates of CO sources with high resolution by adjoint inversion of multiple satellite datasets (MOPITT, AIRS, SCIAMACHY, TES), *Atmos. Chem. Phys*, *10*(3), 855–876, doi:10.5194/acp–10–855–2010.

Krol, M., S. Houweling, B. Bregman, M. van den Broek, A. Segers, P. van Velthoven, W. Peters, F. Dentener, and P. Bergamaschi (2005), The two-way nested global chemistry-transport zoom model TM5: Algorithm and applications, *Atmos. Chem. Phys*, *5*(2), 417–432, doi:10.5194/acp–5–417–2005.

Langenfelds, R. L., R. J. Francey, B. C. Pak, L. P. Steele, J. Lloyd, C. M. Trudinger, and C. E. Allison (2002), Interannual growth rate variations of atmospheric CO_2 and its $\delta^{13}C$, H_2, CH_4, and CO between 1992 and 1999 linked to biomass burning, *Global Biogeochem. Cycles*, *16*(3), 1048, doi:10.1029/2001GB001466.

Lallo, M., T. Aalto, T. Laurila, and J. Hatakka (2008), Seasonal variations in hydrogen deposition to boreal forest soil in southern Finland, *Geophys. Res. Lett*, *35*, L04402, doi:10.1029/2007GL032357.

Mar, K. A., M. C. McCarthy, P. Connell, and K. A. Boering (2007), Modeling the photochemical origins of the extreme deuterium enrichment in stratospheric H_2, *J. Geophys. Res*, *112*, D19302, doi:10.1029/2006JD007403.

McCarthy, M. C., K. A. Boering, T. Rahn, J. Eiler, A. Rice, S. C. Tyler, and E. Atlas (2004), The hydrogen isotopic composition of water vapor entering the stratosphere inferred from high precision measurements of δD-CH_4 and δD-H_2, *J. Geophys Res*, *109*, D07304, doi:10.1029/2003JD004003.

Meirink, J. F., et al. (2008a), Four-dimensional variational data assimilation for inverse modelling of atmospheric methane emissions: Analysis of SCIAMACHY observations, *J. Geophys. Res*, *113*, D17301, doi:10.1029/2007JD009740.

Meirink, J. F., P. Bergamaschi, and M. C. Krol (2008b), Four-dimensional variational data assimilation for inverse modelling of atmospheric methane emissions: Method and comparison with synthesis inversion, *Atmos. Chem. Phys*, *8* (21), 6341–6353, doi: 10.5194/acp–8–6341–2008.

Müller, J.-F. (1992), Geographical distribution and seasonal variation of surface emissions and deposition velocities of atmospheric trace gases, *J. Geophys. Res*, *97*(D4), 3787–3804, doi:10.1029/91JD02757.

Noije, T. P. C. v., H. J. Eskes, M. v. Weele, and P. F. J. v. Velthoven (2004), Implications of the enhanced Brewer-Dobson circulation in European Centre for Medium-Range Weather Forecasts reanalysis ERA-40 for the stratosphere-troposphere exchange of ozone in global chemistry transport models, *J. Geophys. Res*, *109*, D19308, doi:10.1029/2004JD004586.

Novelli, P. C., P. M. Lang, K. A. Masarie, D. F. Hurst, R. Myers, and J. W. Elkins (1999), Molecular hydrogen in the troposphere: Global distribution and budget, *J. Geophys. Res*, *104*(D23), 30427–30444, doi:10.1029/1999JD900788.

Patra, P. K., et al. (2008), TransCom model simulations of hourly atmospheric CO_2: Analysis of synoptic-scale variations for the period 2002-2003, *Glob. Biogeochem. Cycl*, *22*, GB4013, doi: 10.1029/2007GB003081.

Pieterse, G., M. C. Krol, and T. Röckmann (2009), A consistent molecular hydrogen isotope chemistry scheme based on an independent bond approximation, *Atmos. Chem. Phys*, *9*, 8503–8529, doi:10.5194/acp–9–8503–2009.

Pieterse, G., M. C. Krol, A. M. Batenburg, L. P. Steele, P. B. Krummel, R. L. Langenfelds, and T. Röckmann (2011), Global modelling of H_2 mixing ratios and isotopic compositions with the TM5 model, *Atmos. Chem. Phys*, *11*(14), 7001–7026, doi:10.5194/acp–11–7001–2011.

Pison, I., P. Bousquet, F. Chevallier, S. Szopa, and D. Hauglustaine (2009), Multi-species inversion of CH_4, CO and H_2 emissions from surface measurements, *Atmos. Chem. Phys*, *9*(14), 5281–5297, doi:10.5194/acp–9–5281–2009.

Popa, M. E., A. T. Vermeulen, W. C. M. van den Bulk, P. A. C. Jongejan, A. M. Batenburg, W. Zahorowski, and T. Röckmann (2011), H_2 vertical profiles in the continental boundary layer: Measurements at the Cabauw tall tower in The Netherlands, *Atmos. Chem. Phys*, *11*(13), 6425–6443, doi:10.5194/acp–11–6425–2011.

Price, H., L. Jaeglé, A. Rice, P. Quay, P. C. Novelli, and G. R. (2007), Global budget of molecular hydrogen and its deuterium content: Constraints from ground station, cruise, and aircraft observations, *J. Geophys. Res*, *112*, D22108, doi:10.1029/2006JD008152.

Pul, W. A. J. v., and A. F. G. Jacobs (1994), The conductance of a maize crop and the underlying soil to ozone under various environmental conditions, *Bound.-Lay. Meteorol*, *69*(1), 83–99, doi:10.1007/BF00713296.

Rahn, T., N. Kitchen, and J. M. Eiler (2002), D/H ratios of atmospheric H_2 in urban air: Results using new methods for analysis of nano-molar H_2 samples, *Geochim. Cosmochim. Acta*, *66*, 2475–2481, doi:10.1016/S0016–7037(02)00858–X.

Rahn, T., J. M. Eiler, K. A. Boering, P. O. Wennberg, M. C. McCarthy, S. Tyler, S. Schauffler, S. Donnelly, and E. Atlas (2003), Extreme deuterium enrichment in stratospheric hydrogen and the global atmospheric budget of H_2, *Nature*, *424*, 918–921, doi:10.1038/nature01917.

Rhee, T. S., C. A. M. Brenninkmeijer, and T. Röckmann (2006), The overwhelming role of soils in the global atmospheric hydrogen cycle, *Atmos. Chem. Phys*, *6*, 1611–1625, doi:10.5194/acp–6–1611–2006.

Rice, A., P. Quay, J. Stutsman, R. Gammon, H. Price, and L. Jaeglé (2010), Meridional distribution of molecular hydrogen and its deuterium content in the atmosphere, *J. Geophys. Res*, *115*, D12306, doi:10.1029/2009JD012529.

Röckmann, T., T. S. Rhee, and A. Engel (2003), Heavy hydrogen in the stratosphere, *Atmos. Chem. Phys*, *3*, 2015–2023, doi: 10.5194/acp–3–2015–2003.

Sander, S. P., et al., (2006), Chemical kinetics and photochemical data for use in atmospheric studies, evaluation number 15, *Technical report, JPL Publication 06-2*, Jet Propulsion Laboratory, Pasadena.

Sanderson, M. G., W. J. Collins, R. G. Derwent, and C. E. Johnson (2003), Simulation of global hydrogen levels using a Lagrangian three dimensional model, *J. Atmos. Chem*, *46* (1), 15–28, doi:10.1023/A:1024824223232.

Schaap, M., M. Roemer, F. Sauter, G. Boersen, R. Timmermans, A. T. Vermeulen, and P. J. H. Builtjens, (2005), LOTOS-EUROS: Documentation, *Technical report*, Netherlands Organisation for Applied Scientific Research (TNO), Apeldoorn, The Netherlands.

Schultz, M. G., and O. Stein, (2006), GEMS (GRG) emissions for 2003 reanalysis simulations, *Technical report*, MPI-M.

Schultz, M. G., T. Diehl, G. P. Brasseur, and W. Zittel (2003), Air pollution and climate-forcing impacts of a global hydrogen economy, *Science*, *302*(5645), 624–627, doi:10.1126/science.1089527.

Schultz, M. G. et al., (2007), REanalysis of the TROpospheric chemical composition over the past 40 years (RETRO)—A long-term global modeling study of tropospheric chemistry, Technical report, Max Planck Institute for Meteorology, Jülich/Hamburg, Germany.

Tromp, T. K., R.-L. Shia, M. Allen, J. M. Eiler, and Y. L. Yung (2003), Potential environmental impact of a hydrogen economy on the stratosphere, *Science*, *300*(5626), 1740–1742, doi:10.1126/science.1085169.

Villani, M. G., P. Bergamaschi, M. C. Krol, J. F. Meirink, and F. Dentener (2010), Inverse modeling of European CH4 emissions: Sensitivity to the observational network, *Atmos. Chem. Phys*, *10*, 1249–1267, doi:10.5194/acp–10–1249–2010.

Vogel, B., T. Feck, J.-U. Grooß, and M. Riese (2012), Impact of a possible future global hydrogen economy on arctic stratospheric ozone loss, *Energy Environ. Sci*, *5*(4), 6445–6452, doi:10.1039/C2EE03181G.

Vollmer, M. K., S. Walter, J. Mohn, M. Steinbacher, S. W. Bond, T. Röckmann, and S. Reimann (2012), Molecular hydrogen (H_2) combustion emissions and their isotope (*D*/*H*) signatures from domestic heaters, diesel vehicle engines, waste incinerator plants, and biomass burning, *Atmos. Chem. Phys*, *12*(3), 6275–6289, doi: 10.5194/acp-12-6275-2012.

Warwick, N. J., S. Bekki, E. G. Nisbet, and J. A. Pyle (2004), Impact of a hydrogen economy on the stratosphere and troposphere studied in a 2D model, *Geophys. Res. Lett*, *31*, L05107, doi:10.1029/2003GL019224.

Werf, G. R. v. d., J. T. Randerson, G. J. Collatz, and L. Giglio (2003), Carbon emissions from fires in tropical and subtropical ecosystems, *Glob. Change Biol*, *9*, 547–562, doi:10.1046/j.1365–2486.2003.00604.x.

Werf, G. R. v. d., J. T. Randerson, L. Giglio, G. J. Collatz, M. Mu, P. S. Kasibhatla, D. C. Morton, R. S. DeFries, Y. Jin, and T. T. v. Leeuwen (2010), Global fire emissions and the contribution of deforestation, savanna, forest, agricultural, and peat fires (1997–2009), *Atmos. Chem. Phys*, *10*(23), 11707–11735, doi:10.5194/acp–10–11707–2010.

Xiao, X., et al. (2007), Optimal estimation of the soil uptake of molecular hydrogen from the advanced global atmospheric gases experiments and other measurements, *J. Geophys. Res*, *112*, D07303, doi:10.1029/2006JD007241.

Yashiro, H., K. Sudo, S. Yonemura, and M. Takigawa (2011), The impact of soil uptake on the global distribution of molecular hydrogen: Chemical transport model simulation, *Atmos. Chem. Phys*, *11*, 6701–6719, doi:10.5194/acp–11–6701–2011.

Yonemura, S., S. Kawashima, and H. Tsuruta (2000), Carbon monoxide, hydrogen, and methane uptake by soils in a temperate arable field and a forest, *J. Geophys. Res*, *105* (D11), 14347–14362, doi:10.1029/1999JD901156.

Yver, C., M. Schmidt, P. Bousquet, W. Zahorowski, and M. Ramonet (2009), Estimation of the molecular hydrogen soil uptake and traffic emissions at a suburban site near Paris through hydrogen, carbon monoxide, and radon-222 semicontinuous measurements, *J. Geophys. Res*, *114*, D18304, doi:10.1029/2009JD012122.

Yver, C. E., et al. (2011), A new estimation of the recent tropospheric molecular hydrogen budget using atmospheric observations and variational inversion, *Atmos. Chem. Phys*, *11*(7), 3375–3392, doi:10.5194/acp–11–3375–2011.